ELSEVIER

Contents lists available at ScienceDirect

# Gas Science and Engineering

journal homepage: www.journals.elsevier.com/gas-science-and-engineering



# High-pressure vapor-liquid equilibrium measurements of methane + water mixtures by nuclear magnetic resonance spectroscopy

Samantha L. Miller <sup>a,c</sup>, Michael Sartini <sup>b,c</sup>, Bret C. Windom <sup>b</sup>, Christopher L. Suiter <sup>c</sup>, Mark O. McLinden <sup>c</sup>, Nancy E. Levinger <sup>a,d</sup>, Jason A. Widegren <sup>c,\*</sup>

- <sup>a</sup> Department of Chemistry, Colorado State University, 1872 Campus Delivery, Fort Collins, CO, 80523-1872, USA
- b Department of Mechanical Engineering, Colorado State University, 1374 Campus Delivery, Fort Collins, CO, 80523-1370, USA
- c Applied Chemicals and Materials Division, National Institute of Standards and Technology, 325 Broadway, Boulder, CO, 80305-3328, USA
- d Department of Electrical and Computer Engineering, Colorado State University, 1373 Campus Delivery, Fort Collins, CO, 80523-1373, USA

#### ARTICLE INFO

#### Keywords: Vapor-liquid equilibrium (VLE) Methane and water mixture Nuclear magnetic resonance (NMR) spectroscopy REFPROP

GERG-2008 natural gas model

#### ABSTRACT

The vapor-liquid equilibrium (VLE) of methane + water mixtures has been studied with nuclear magnetic resonance (NMR) spectroscopy. This work had two primary goals. The first goal was to develop methods that broaden the utility of NMR spectroscopy for VLE measurements. In this regard, we report a method by which the liquid-phase and vapor-phase compositions are measured in separate experiments by adjusting the height of the liquid phase in the sample tube. We also report a method for hastening phase equilibration by adding glass beads to the sample and repeatedly inverting the sample tube. The second goal of this work was to collect VLE data on a challenging mixture with real-world importance. Mixtures of methane + water are a useful test case because of their challenging characteristics, including the widely differing vapor pressures of the two components. One use for accurate VLE data on methane + water mixtures is to better predict the formation of harmful liquid phases in natural gas pipelines. Herein we utilize <sup>1</sup>H NMR spectroscopy to measure the VLE of methane + water mixtures at temperatures of 299.73, 307.98, and 323.25 K, and pressures ranging from 0.69 MPa to 13.89 MPa. Experiments were carried out with a 600 MHz spectrometer. Mixtures were prepared and equilibrated in a highpressure zirconia sample tube with an integrated needle valve. NMR-based VLE measurements on the liquid phase are in good agreement with available literature data and with Henry's Law predictions at low pressures. However, the commonly used GERG-2008 model for natural gas systems deviates dramatically from the experimental data for the liquid phase. NMR-based VLE measurements on the vapor-phase resulted in measured water concentrations that are systematically lower than available literature data and models. This systematic offset is likely caused by peak overlap in the NMR spectra.

# 1. Introduction

The condensation of lower-volatility components, such as heavy hydrocarbons and water, from natural gas is a serious concern in the operation of pipelines and other infrastructure (Menon et al., 2017; Jafar Mazumder, 2020; Popoola et al., 2013; Kidnay and Parrish, 2006). Condensation can lead to corrosion (Jafar Mazumder, 2020; Popoola et al., 2013; Tamalmani and Husin, 2020) and even slugs of liquid in a pipeline, (Shi et al., 2021) with potentially disastrous consequences should a liquid slug enter a compressor station (Kidnay and Parrish, 2006). Natural gas is processed near the wellhead to meet moisture and dewpoint specifications, and the dewpoint of pipeline gas is routinely

monitored with industry-standard techniques, such as the chilled mirror (Sharanik et al., 2023).

The dewpoint of a gas mixture is the state at which condensation first occurs, and it can be predicted by comprehensive thermodynamic mixture models. Such models are largely empirical and are developed by fitting experimental data. Vapor-liquid equilibrium (VLE) data comprise measurements of temperature (T), pressure (p), liquid-phase composition (x), and vapor-phase composition (y) for the two phases in thermodynamic equilibrium. VLE encompasses both dewpoint measurements (i.e., T, p, y of the vapor phase in equilibrium with a small quantity of liquid) and bubble-point measurements (i.e., T, p, x of the liquid phase in equilibrium with a small quantity of vapor). VLE

E-mail address: jason.widegren@nist.gov (J.A. Widegren).

<sup>\*</sup> Corresponding author.

measurements capture much of the nonideality in the mixture behavior and are, thus, important data needed to determine the mixture parameters for thermodynamic models.

Many different thermodynamic mixture models have been used to predict the properties of natural gas (Hall and Yarborough, 1973). The current ISO standard for natural gas mixtures is the GERG-2008 mixture model (Kunz and Wagner, 2012; Herrig, 2018; Lemmon). As such, it is a primary point of comparison for our experimental results. A potential weakness of the GERG-2008 model is that it was developed primarily with vapor-phase data. Therefore, good VLE data for mixtures of light hydrocarbons and water could allow for improvements in the GERG-2008 model for the prediction of aqueous condensate formation. The GERG-2008 model, like most multi-component mixture models, is based on the behavior of the constituent binary pairs (Hughes et al., 2017). Thus, in this work, we measure the VLE of methane + water mixtures. A follow-on effort on mixtures of ethane + water and propane + water is presently underway.

The mixture of methane + water presents multiple challenges for VLE measurements, which explains the current lack of low-uncertainty VLE data in the literature on this important system. First, the two compounds have very different volatilities, which means that, in the vapor phase, the mole fractions of the two compounds differ by several orders of magnitude at industrially relevant pressures (Rigby and Prausnitz, 1968). Similarly, the solubility of methane in water is very low, (Cosgrove and Walkley, 1981; Wilhelm et al., 1977) which means there is also a large concentration mismatch in the liquid phase. Accurately analyzing mole ratios for mixtures with large concentration differences is inherently difficult. Additionally, few analytical techniques are capable of simultaneous, low-uncertainty analysis of both water and methane. Gas chromatography with flame-ionization detection (GC-FID), which is widely used to determine phase composition for VLE measurements, (Hughes et al., 2017; Suiter et al., 2020; Frost et al., 2014; Mohammadi et al., 2006; Richon et al., 2005) is not sensitive to water. GC with a thermal conductivity detector (GC-TCD) can be used, (Frost et al., 2014; Mohammadi et al., 2006) but it has relatively poor sensitivity and a small linear response range, (Budiman et al., 2015) which are both problematic characteristics given the large difference in concentration between the two components. For any mixture, extracting GC samples from a pressurized, equilibrated sample cell is fraught with difficulties (Richon et al., 2005; Chapoy et al., 2005). The mixture of methane + water is especially challenging because of the combination of the large difference in vapor pressure, water's tendency to adsorb onto surfaces, which is particularly troublesome for the low-concentration vapor phase, and methane's tendency to leak (Frost et al., 2014). On top of that, the nonpolar-polar nature of the two components results in significantly nonideal mixture behavior under most conditions, so simplifying assumptions, such as Raoult's law or Henry's law, cannot be made over a wide range of temperatures or pressures.

In an effort to overcome such difficulties, we recently developed a new method for VLE measurements that is based on nuclear magnetic resonance (NMR) spectroscopy (Suiter et al., 2020). NMR is radiofrequency spectroscopy that detects nuclear spins while the sample is held in a magnetic field (Claridge, 2009). Conveniently, <sup>1</sup>H, which is present in both methane and water, is arguably the best nucleus for quantitative NMR studies for two reasons (Suiter et al., 2020). First, it is relatively easy to implement spectral acquisition parameters that result in each <sup>1</sup>H signal being proportional to the number of nuclei that gives rise to it. This "equal sensitivity" property of <sup>1</sup>H NMR spectroscopy is a key advantage for VLE measurements because it allows for the direct determination of mole ratios in mixtures by simple comparison of peak areas. Second, <sup>1</sup>H affords relatively large signals. This is important for the present study because, even though NMR spectroscopy has a wide linear response range, (Sotak et al., 1983) the small signal from the minor component (water in the vapor phase or methane in the liquid phase) necessitates signal averaging to achieve quantifiable signal areas. And, even then, new integration protocols had to be developed for these small signals, as detailed in Section 2.5.

Another key advantage of NMR spectroscopy for VLE measurements is that there is no need to withdraw samples for analysis because compositions are determined *in situ* with the methane + water mixture in a sealed sample cell. Thus, once thermodynamic equilibrium is established, it is not disturbed by sampling. This advantage was a major motivation for the development of NMR spectroscopy as a VLE measurement tool (Suiter et al., 2020).

Some of the limitations of NMR spectroscopy are also highlighted in the current work. Unlike chromatographic methods, the peaks in the NMR spectrum cannot be moved around by changing experimental parameters; therefore, peak overlap can complicate signal integration. Additionally, the presence of a strong magnetic field complicates the measurement of temperature and pressure (Suiter et al., 2020). Furthermore, the geometry of sample cells used in NMR spectroscopy—narrow tubes with an inner diameter of a few millimeters—impedes phase equilibration because of the small liquid-vapor interface. Consequently, assuring complete phase equilibration in the sample cell is a point of emphasis for this study.

Herein we report the results of a new method, based on <sup>1</sup>H NMR spectroscopy, for *in situ* VLE measurements of hydrocarbon + water mixtures. We report VLE data for mixtures of methane + water at pressures ranging from 0.69 MPa to 13.89 MPa and temperatures of 299.73 K, 307.98 K, and 323.25 K. These conditions are at the higher end of ambient temperatures and more than cover the pressure range of natural gas transmission pipelines.

#### 2. Materials and methods

#### 2.1. Materials

Methane (CH<sub>4</sub>) with a purity of 99.999 % (by volume) was purchased from a commercial source and used without further purification. Ultrapure water with a conductivity of  $\leq$ 0.055 µS/cm, (resistivity of  $\geq$ 18.0 M $\Omega$ ·cm) was prepared in-house with a commercial filtration and purification system. <sup>1</sup>H NMR spectroscopy was used to verify the purity of both the water and methane used in this work.

#### 2.2. NMR spectrometer and sample cell

The most commonly used NMR sample cells are thin-walled borosilicate glass tubes sealed with a plastic cap. Such cells are not suitable for high pressures or gaseous samples. For this study, the NMR sample cell consisted of an yttria-stabilized zirconia ceramic tube with an integrated needle valve from Daedalus Innovations  $^1$  (Aston, PA), Fig. 1. With the needle valve closed, the cell had an internal volume of 1.011 mL. The zirconia tube had a length of 92 mm, an I.D. of 3.6 mm, an O.D. of 5.0 mm, and a pressure rating of 100 MPa. The seal between the zirconia tube and the aluminum manifold was made with a Viton O-ring. Tests with methane gas confirmed that, with the needle valve closed, this system could hold pressure for weeks without detectable leakage by  $^1\mathrm{H}$  NMR spectroscopy (i.e., there was no decline in the CH4 peak intensity).

All experiments were conducted with a 600 MHz NMR spectrometer with a double-resonance NMR probe (Bruker Corporation, UltraShield magnet, Avance III console). The spectroscopically active portion of the NMR tube (the "spectral window") extends from about 13 mm to 25 mm above the bottom of the NMR tube. This instrument uses a flow of conditioned nitrogen gas around the sample tube to control the sample

<sup>&</sup>lt;sup>1</sup> Certain trade names and products are given to adequately document the experimental equipment and procedures. This does not constitute a recommendation or endorsement of these products by the National Institute of Standards and Technology, nor does it imply that the products are necessarily the best available for the purpose.

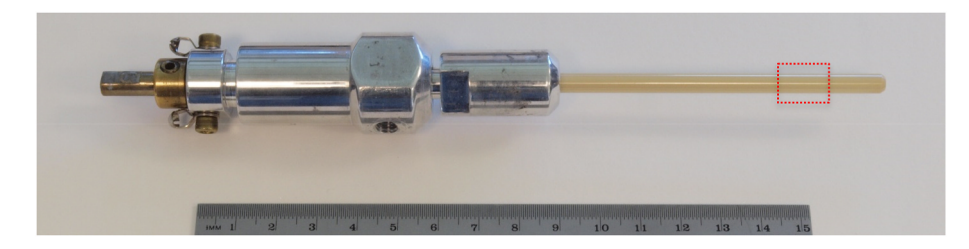
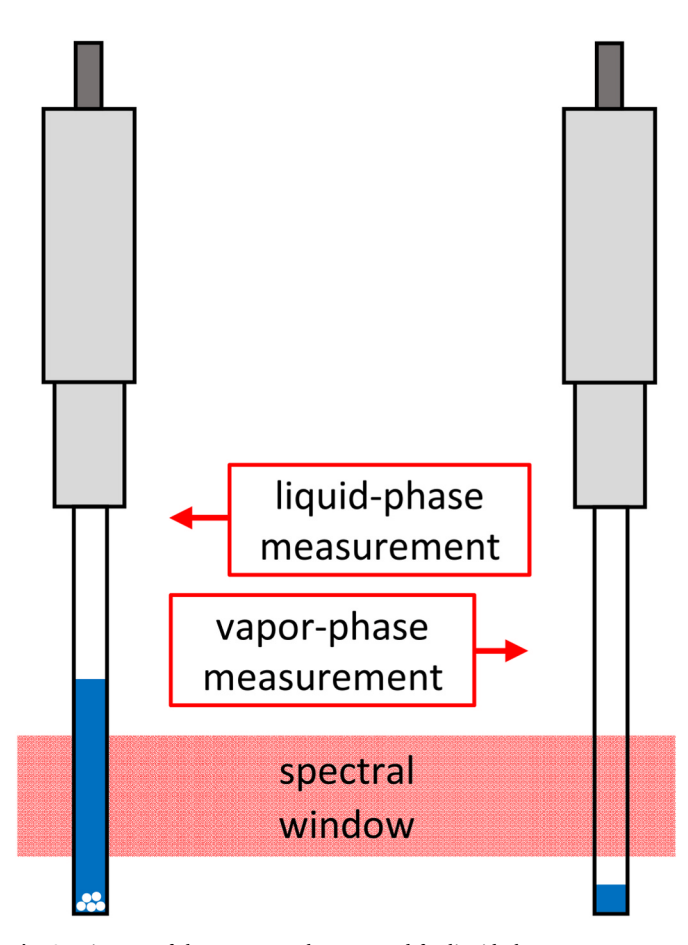


Fig. 1. NMR sample cell used in this work with a centimeter scale to indicate size. Liquid water was added to the zirconia tube (right) and pressurized with methane through transfer lines connected to the aluminum needle valve (left). The dashed red box indicates the location of the spectral window for the cell.

temperature. Because the gas flow rate and the geometry of the sample cell influence the sample temperature, a calibrated temperature sensor was used to select setpoint + flowrate combinations that corresponded to the desired sample temperatures (see Section 2.6.).

#### 2.3. Mixture preparation

The high surface tension of water prevented the use of our previously developed (Suiter et al., 2020) method of creating a thin, high-surface-area, suspended liquid phase by means of a capillary insert, which allowed for simultaneous measurement of liquid- and vapor-phase compositions. Consequently, for each temperature-pressure state point, two samples were prepared, Fig. 2. A "vapor-phase" sample was prepared in which the liquid phase extended only about 5 mm above



**Fig. 2.** Diagram of the NMR samples prepared for liquid-phase measurements (left) or vapor-phase measurements (right). The height of the liquid phase (shown in blue) determined whether the liquid phase or the vapor phase of the sample filled the spectral window of the NMR spectrometer (shaded in red). The borosilicate glass beads (white circles) used to mix the liquid phase were below the spectral window during the NMR measurements.

the bottom of the NMR tube and, therefore, was below the spectral window of the instrument. Thus, for a vapor-phase sample, only signals from the vapor phase were observed in the NMR spectrum. A second "liquid-phase" sample was prepared with a liquid phase that extended about 45 mm above the bottom of the NMR tube, which is approximately 10 mm above the top of the instrument's spectral window. Thus, for a liquid-phase sample, only signals from the liquid phase were observed in the NMR spectrum. The liquid-phase sample also contained 10 glass beads (borosilicate, 2.23 g/cm³ density, 1 mm diameter), which facilitated equilibration, as discussed in Section 2.4. During spectroscopic measurements, the glass beads rested at the bottom of the liquid phase and outside the spectral window (Fig. 2); thus, the beads did not affect the spectra.

Vapor-phase samples were prepared by adding approximately 20 mg of degassed water to the NMR tube. Liquid-phase samples were prepared by adding 10 glass beads (1 mm diameter) and approximately 390 mg of degassed water to the NMR tube. Methane was then added to the NMR cell using a high-pressure manifold, shown in Fig. 3 (a photograph of the manifold is available as Fig. S6 in Appendix A). Prior to attaching the NMR cell, the manifold was evacuated for 5 min with valves 2 and 6 closed. The NMR sample cell was then connected and evacuated for 30 s with valves 4 and 6 closed. Following this, the sample cell (still attached to the manifold via a 30 cm length of 1.5875 mm OD stainless-steel tubing) was placed in a nitrile glove (to keep it dry) and immersed in a constant-temperature water bath that was set to the target temperature of the experiment. The sample cell was then slowly pressurized with methane directly from the methane cylinder (with valves 1, 4 and 5 closed) or from the high-pressure syringe pump (with valves 1 and 6 closed). The sample cell remained in the water bath and the pressure was monitored for at least two more minutes. During this time, methane was added to the sample cell as necessary to maintain the desired pressure. After the pressure had stabilized, the sample pressure was recorded, and the needle valve on the sample cell was closed, which sealed the mixture in the cell. The sample cell was weighed at every step of the mixture preparation, so the masses of added water and methane were known; these values were needed to make a pressure correction due to phase equilibration (see Section 2.7.).

# 2.4. Equilibration procedure for liquid-phase samples

A mixing procedure hastened equilibration of liquid-phase samples. As mentioned in Section 2.3, glass beads were added to liquid-phase samples. These beads were used to mix the liquid phase by use of a custom device comprising a rotating arm inside a temperature-controlled environmental chamber. This apparatus, shown in Fig. 4, utilizes a micro-controller, stepper motor, two sample-holding brackets, and a timing pully to allow for automated rotation of NMR sample cells at reproducible angles. The equilibration protocol began by inserting the NMR sample cell into a plastic tube and plugging the ends of the tube with insulation. The tube was mounted on one of the brackets on the rotating arm (with the NMR sample cell in an upright position). The environmental chamber (Thermotron, model s-8-8200) was set to the desired temperature and then automated rotation of the sample cell commenced. The temperature setting in the environmental chamber was

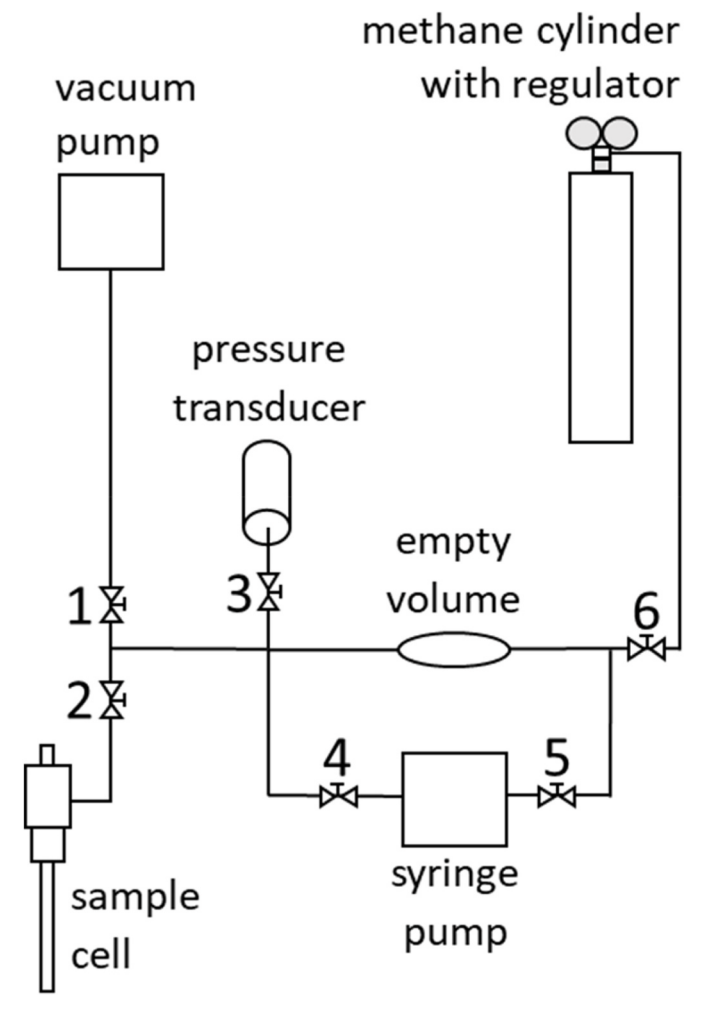


**Fig. 3.** Diagram of high-pressure manifold used for VLE sample preparation. Numbers refer to valves mentioned in the text.

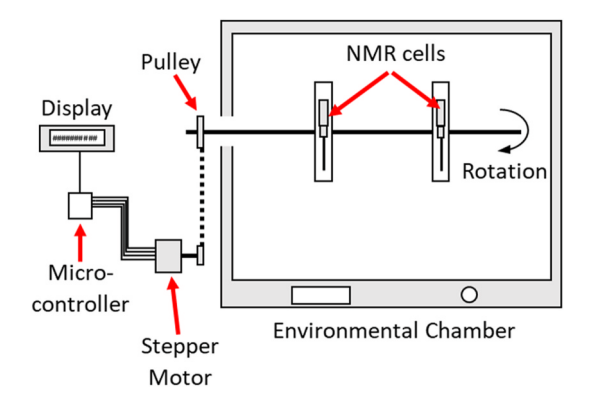


**Fig. 4.** Diagram of the device used to equilibrate liquid-phase samples. Photographs of this device are available as Figs. S8–S10 in Appendix A.

determined with the same PRT that was used in the constant-temperature water bath (see Section 2.3.). Temperature gradients in the environmental chamber were a significant source of uncertainty in the equilibration temperature (see Table S1 of the Supporting Information for details). The arm was set to rotate the sample cell 180° (i.e., upside down), pause for 5 s (to allow time for the glass beads to fall to the "top" of the liquid phase), rotate another 180° (i.e., its original upright position), pause for 5 s (for the glass beads to fall to the bottom of

the liquid phase), and so on. In this manner, the beads moved up and down through the liquid phase and mixed it. Note that the surface tension of water was sufficient to hold the liquid phase in place during the mixing procedure and to hold the glass beads inside the liquid phase (i.e., the liquid phase remained in the end of the sample tube and the beads never crossed the phase boundary into the vapor space). After mixing overnight in this fashion (about 9600 half rotations), the sample cell was removed from the environmental chamber and immediately lowered into the NMR spectrometer, which had been set to the same temperature as the environmental chamber. During the few seconds of transport, the sample cell remained in the plastic mounting tube to minimize any change in temperature.

#### 2.5. Acquisition and processing of 1H NMR spectra

In the NMR spectrometer's software, a temperature setting was selected that corresponded to the desired sample temperature (see Section 2.6 for more details on how these settings were determined). The sample cell was lowered into the spectrometer with a non-magnetic chain connected to the top of the sample cell. With the sample in place, the NMR probe was tuned and matched to the <sup>1</sup>H frequency. Manual shimming (i.e., fine adjustment of the magnetic field) was applied to achieve good peak shapes and maximize the signal-to-noise ratio; automatic shimming routines were not used because of the lack of deuterium in these samples. For each sample, an inversion-recovery pulse sequence was used to determine the  $T_1$  relaxation time for each NMR signal. Then the pulse delay for spectral acquisition was set to at least 5  $T_1$  for the slowest decaying signal to ensure quantitative peak integrals (a typical pulse delay was 75 s) (Suiter et al., 2019). A high-power 90° pulse of 10.875 µs was used. For liquid-phase spectra, an acquisition time of 5.45 s and a dwell time of 41.6  $\mu s$  were used (resulting in 128k points collected and a digital resolution of 0.0459 Hz). For vapor-phase spectra, an acquisition time of 10.9 s and a dwell time of 83.2 µs were used (resulting in 128k points collected and a digital resolution of 0.0459 Hz). All spectra were collected with a spectral width of 10 ppm and an offset frequency of 3 ppm. This offset frequency is approximately equidistant from the water and methane peaks, ensuring equal excitation of the two signals (Suiter et al., 2019). For liquid-phase samples, 32 scans were acquired; for vapor-phase samples, 256 scans were acquired. With these parameters, the total period to collect a liquid-phase spectrum was about 45 min (the limiting signal was from dissolved methane). The total period to collect a vapor-phase spectrum was about 6 h (the limiting signal was from water vapor).

Data processing for all spectra began by zero-filling to double the number of collected data points. Exponential line broadening of 0.3 Hz was applied to all liquid-phase spectra. To increase the signal-to-noise ratio, exponential line broadening of 3–15 Hz was applied to all vapor-phase spectra. The data were manually phased and then a multipoint baseline correction was done by manually selecting baseline points far from the peaks, then correcting with an ablative function.

For liquid phase spectra, the signal-to-noise ratio for the methane peak ranged from 56 (at the lowest pressure and highest temperature) to 1168 (at the highest pressure and lowest temperature), and the full width at half maximum intensity (FWHM or "linewidth") for the methane peak ranged from 4.2 Hz to 6.6 Hz. For the vapor phase spectra, the signal-to-noise ratio for the water peak ranged from 6810 (at the lowest pressure and highest temperature) to 7.5 (at the highest pressure and lowest temperature), and the FWHM for the water peak ranged from 6.6 Hz to 18.9 Hz after line broadening.

# 2.5.1. Integration of the liquid-phase spectra

Methane and water signals in the liquid-phase spectra were integrated numerically using the same general strategy that we reported previously (Suiter et al., 2019). The linewidth (FWHM) for each peak was determined. Then integral limits for each peak were set at  $\pm 30$  FWHM. The choice of 30 FWHM represents a compromise in which a

high percentage of each peak's intensity is within the integral limits (98.9 %, assuming a perfectly Lorentzian peak shape) but the overlap correction is still reasonably small. Integration of the spectra with integral limits from  $\pm 5$  FWHM to  $\pm 85$  FWHM results in a plateau in the final (corrected) mole fractions when integral limits are between  $\pm 30$ FWHM and  $\pm 50$  FWHM, which suggests that the assumption of Lorentzian peak shape works best in this range. After integration, a correction was applied in which the overlapping intensity of the large water peak on the methane integral region was subtracted (Suiter et al., 2019). At the lowest pressures (nominally 0.7 MPa), this overlap correction is about 30 % of the methane peak's (uncorrected) intensity, despite the seemingly good peak separation. However, the relative importance of the overlap correction drops rapidly for higher pressures because the size of the methane peak increases while the size of the correction remains roughly constant. At the highest pressures the overlap correction is only about 3 % of the methane peak's (uncorrected) intensity. The overlapping intensity of the small methane peak on the water integral region is negligibly small, so no correction was needed.

#### 2.5.2. Integration of the vapor-phase spectra

The spectral linewidth for each peak was determined. The large methane-vapor peak was integrated with limits set at  $\pm 30$  FWHM, which encompasses the small water-vapor peak (the corrected water peak area was later subtracted from the corrected methane peak area). Next, integration of the water-vapor peak began with an additional baseline subtraction to flatten the sloping shoulder of the methane-vapor peak in the vicinity of the water-vapor peak. To obtain a reliable fit of the sloping "baseline" for the subtraction, baseline points very close to the water-vapor peak had to be selected. In practice, this baseline subtraction was done with a cubic splines function fitted to a multipoint baseline selection that included baseline points at  $\pm 3$  FWHM for the water-vapor peak. The water-vapor peak was then integrated with limits set at  $\pm 3$  FWHM; thus, the closest "baseline" points exactly matched the edges of the integrated region.

The additional baseline subtraction in the vicinity of the water-vapor peak removes the overlapping intensity of the methane-vapor peak. Two other corrections to peak intensity were also applied. First, since different numbers of linewidths were used to integrate the methane and water peaks, a correction was made to account for the differing percentage of peak intensity that was captured for each (Suiter et al., 2019). Second, picking baseline points so near the integrated region results in a significant subtraction of peak intensity inside the integrated region, as shown in Fig. 5. It removes the shoulders of the peak (i.e., the peak intensity outside the integrated region), but it also removes some of the peak intensity inside the integrated region by cutting off the base of the peak. Assuming a Lorentzian lineshape, one can calculate that selecting baseline points at  $\pm 3$  FWHM results in a loss of 10.3 % of the peak intensity inside the integrated region of  $\pm 3$  FWHM. Hence, a correction to the integrated area of the water-vapor peak area was made to account for this loss of intensity. Note also that this loss of intensity from baseline flattening rapidly diminishes if baseline points are selected farther from the peak; for example, selecting baseline points as close as  $\pm 15$  FWHM results in a loss of only 2.1 % of the intensity and selecting baseline points as close as  $\pm 100$  FWHM results in a loss of only 0.32 % of the intensity.

#### 2.5.3. Uncertainty in the composition measurement

Integration of the liquid- and vapor-phase spectra had four significant sources of uncertainty: manual phasing of the spectra ( $u_{\rm phase}$ ), baseline subtraction/flattening ( $u_{\rm baseline}$ ), the corrections based on linewidths integrated ( $u_{\rm lw}$ ), and incomplete relaxation of spins between rf pulses ( $u_{\rm TI}$ ). Two sources of uncertainty identified previously, (Suiter et al., 2019) namely uncertainty from nonuniform excitation of spins and uncertainty from digital resolution, were not significant in the present work and were ignored. The value of  $u_{\rm phase}$  and  $u_{\rm TI}$  were

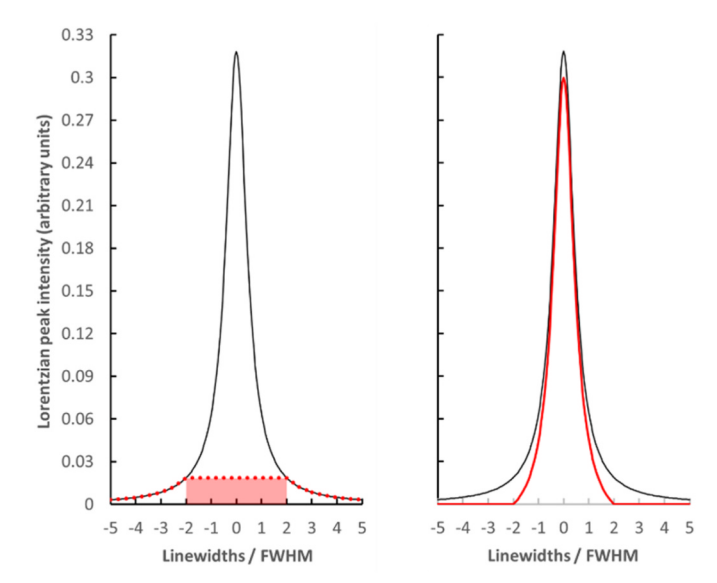


**Fig. 5.** Schematic showing how baseline flattening very near the peak results in a significant subtraction of peak intensity underneath the peak (i.e., in the integrated region). The left side shows the original Lorentzian peak (solid black line) along with the baseline subtraction function (dotted red line) that is generated with a multipoint baseline correction to within  $\pm 2$  FWHM. The shaded red rectangle (left) shows the area under the peak that is subtracted. The right side shows the original Lorentzian peak (solid black line) along with the peak that results from the baseline flattening procedure (solid red line).

determined as previously reported (Suiter et al., 2019). The value of  $u_{\rm baseline}$  at each nominal pressure was estimated from the average difference in signal integration with two different baseline subtraction methods: an ablative baseline subtraction that worked well for these spectra, or a polynomial baseline subtraction that made an obviously poorer correction. Similarly, the value of  $u_{\rm lw}$  was estimated from the average difference in signal integration with integral limits at different multiples of FWHM.

Table 1 shows a complete uncertainty budget for the mole fraction of the minor component in each phase ( $x_{\rm methane}$  and  $y_{\rm water}$ ). Uncertainties associated with phasing and baseline flattening were strongly dependent on pressure because the pressure strongly influences the size of the spectral peak for the minor component: higher pressure increases the relative area of the liquid-phase methane peak and decreases the relative area of the vapor-phase water peak. Sample temperature had no obvious influence on the uncertainty in  $x_{\rm methane}$  or  $y_{\rm water}$ , presumably due to its relatively small influence on the size of the peaks. The value of  $u_{\rm lw}$  is relatively large for  $y_{\rm water}$  because of the additional baseline flattening

**Table 1** Uncertainty budget for the mole fraction of the minor component in each phase of the VLE measurement. Combined standard uncertainty ( $u_{\text{combined}}$ ) was calculated by summation in quadrature of the four sources of uncertainty.

Setpoint/MPa	$u_{ m phasing}$	$u_{\mathrm{baseline}}$	$u_{\mathrm{lw}}$	$u_{\mathrm{T1}}$	$u_{ m combined}$
LIQUID-PHASE C	H <sub>4</sub> (x <sub>methane</sub> )				
0.69	15.10%	14.97%	2.37%	0.67%	21.41%
1.73	3.00%	4.98%	2.37%	0.67%	6.31%
3.52	1.07%	2.61%	2.37%	0.67%	3.74%
6.84	0.92%	1.95%	2.37%	0.67%	3.28%
10.32	0.93%	1.22%	2.37%	0.67%	2.90%
13.71	0.91%	1.22%	2.37%	0.67%	2.89%
VAPOR-PHASE H	$I_2O(y_{water})$				
0.76	0.91%	1.22%	8.10%	0.67%	8.27%
1.78	0.93%	1.22%	8.10%	0.67%	8.27%
3.46	0.92%	1.95%	8.10%	0.67%	8.41%
6.97	1.07%	2.61%	8.10%	0.67%	8.60%
10.41	3.00%	4.98%	8.10%	0.67%	9.99%
13.80	15.10%	14.97%	8.10%	0.67%	22.77%

and the very narrow integrals used to integrate that peak. Note that the uncertainty in the mole fraction of the major component in each phase ( $x_{\text{water}}$  and  $y_{\text{methane}}$ ) is negligibly small because it was always very near to unity. That is,  $x_{\text{water}} = 1 - x_{\text{methane}}$ , where  $x_{\text{methane}}$  is three or four orders of magnitude smaller than  $x_{\text{water}}$ , and the uncertainty in the subtraction is even smaller.

#### 2.6. Temperature measurement and uncertainty

The large magnetic field in an NMR spectrometer affects the performance of many types of temperature sensors. The geometric constraints inside an NMR sample tube further limit the choice of sensors (Suiter et al., 2020). Finally, even when working with ambient-pressure samples, it is impractical to have the temperature sensor in place during spectral acquisition because such an arrangement degrades spectral quality.

We chose a "Cernox" thin-film resistance sensor with a cylindrical geometry (Lakeshore Cryotronics, Westerville, OH, "AA" packaging). This type of sensor is free of magnetic materials and is described by the manufacturer as having "low magnetic-field-induced errors". This sensor has a diameter of 3 mm and a length of 8.5 mm. The sensor's four electrical leads were connected to a resistance bridge that was located outside the 5 Gauss line of the spectrometer's magnetic field.

A multipoint calibration curve was used for the Cernox sensor because its resistance is nonlinear with temperature. Two points in the calibration curve were determined with a water triple point cell (273.16 K) and a gallium melting point cell (302.9146 K). The other four points in the calibration curve (nominally 337 K, 327 K, 297 K, and 294 K) were determined by placing the sensor in a thin-walled glass tube and immersing it in a circulating water bath alongside a calibrated platinum resistance thermometer (PRT, standard uncertainty of 0.02 K). The six data points for temperature vs resistance were fitted to a power function (see Fig. S1 of Appendix A), as recommended by the manufacturer. The average deviation of the calibration temperatures from a least-squares fit was 0.36 K.

The calibrated Cernox sensor was then used to measure temperatures and temperature gradients in the NMR spectrometer. This was done by placing the sensor in an empty (i.e., air-filled) zirconia NMR tube. A manifold without an integrated needle valve was used so that the leads for the sensor could pass through the top of the NMR sample cell and out of the spectrometer. The assembled NMR sample cell was then lowered into the spectrometer and allowed to thermally equilibrate. Temperature measurements were made with the tip of the sensor near the bottom or the top of the spectral window (i.e., about 13 mm or 25 mm above the bottom of the NMR tube). Herein, the sample temperature is the average of these two readings, and the temperature gradient is the difference of these two readings.

A calibrated PRT (standard uncertainty of 0.02 K) was used to measure the temperatures and temperature gradients in the oven that was used for overnight equilibration of the liquid-phase samples. Temperatures were determined by placing the PRT in the center of the plastic tube that was used to hold the NMR sample cell inside the oven. The ends of the plastic tube were then plugged with insulation. With the rotation mechanism turned off, the oven temperature at each setpoint was recorded after 30 min of equilibration. Temperature gradients in the oven were measured by placing the bare PRT at locations near the positional extremes caused by rotation of the NMR sample cell.

There are multiple sources of temperature uncertainty for a VLE experiment. First, based on the calibration of the Cernox sensor, the measured temperatures in the NMR cell have a standard uncertainty of 0.36 K. The standard uncertainty due to the temperature gradient in the NMR spectrometer at each setpoint is half of the total gradient; hence, for the lowest to highest setpoints, these standard uncertainties are 0.03 K, 0.01 K, and 0.16 K, respectively. The offset between the temperature in the NMR spectrometer and the equilibration temperature in the oven (including temperature gradients in the oven) is an additional source of

uncertainty for the liquid-phase samples. Estimated standard uncertainties in the equilibration temperature for the lowest to highest setpoints are 0.06 K, 0.16 K, and 0.24 K, respectively. The uncertainty in the PRT used to measure the oven temperature is 0.02 K. Adding these sources of uncertainty in quadrature results in combined standard uncertainties from 0.36 K to 0.46 K; Table S1 in Appendix A details the sources of uncertainty for each phase at each temperature setting.

#### 2.7. Pressure measurement and uncertainty

The pressure of the sample was measured during mixture preparation (see Section 2.3.) immediately before sealing the pressurized NMR sample cell with the needle valve. A calibrated vibrating-quartz-crystal pressure transducer (Paroscientific, Inc., Redmond, WA) with a full-scale pressure of 21.7 MPa was used. This transducer has a standard uncertainty of 0.01 % of full scale, which is 0.0022 MPa.

To determine the experimental pressure of the equilibrated sample (p), the measurement from the pressure transducer  $(p_{\text{transducer}})$  is corrected for the change in sample pressure due to evaporation of water into the vapor phase and the dissolution of methane into the liquid phase after the NMR sample cell was sealed. The correction is calculated as

$$p = (p_{\text{transducer}}) + (p_{\text{transducer}}) \cdot (y_{\text{water}}) - (p_{\text{transducer}}) \cdot [(x_{\text{methane}}) \cdot (mol_{\text{water}}) / (mol_{\text{methane}})]$$
(1)

where (p<sub>transducer</sub>)·(y<sub>water</sub>) adds pressure from water vapor while  $(p_{\text{transducer}}) \cdot [(x_{\text{methane}}) \cdot (mol_{\text{water}}) / (mol_{\text{methane}})]$  subtracts pressure from dissolution of methane. The equilibrated values of  $y_{water}$  and  $x_{methane}$  are determined directly from NMR spectra of the vapor phase and liquid phase, respectively. The equilibrated fraction of total methane that dissolved in the liquid phase is calculated from  $x_{\text{methane}}$ , the total moles of water in the sample (molwater), and the total moles of methane in the sample ( $mol_{methane}$ ). Equation (1) contains multiple approximations. For example, the term  $[(x_{\text{methane}})\cdot (mol_{\text{water}})/(mol_{\text{methane}})]$ , which is used to calculate the fraction of dissolved methane, assumes (in the numerator) that an insignificant fraction of the water evaporates from the liquid phase and (in the denominator) that an insignificant fraction of methane dissolves in the liquid phase. These approximations are relatively minor sources of uncertainty in the pressure correction. The dominant source of uncertainty originates from the unknown level of phase equilibration at the time the NMR cell is sealed (the pressure correction assumes that no phase equilibration has occurred at that point). This is especially problematic given the relatively rapid equilibration of the vapor phase (see Fig. 6). Based on the length of time required to prepare a sample and the observed rate of equilibration for the vapor phase, we estimate a relative standard uncertainty that is 25 % of the magnitude of the

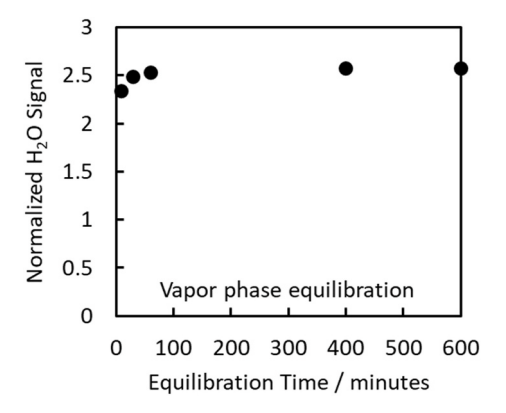


Fig. 6. Equilibration of the vapor phase for a methane + water mixture at 299.73 K and 10.41 MPa. The equilibration took place with the sample cell inside the NMR spectrometer without mechanical mixing. Note that the normalized water vapor signal (i.e., the water vapor signal divided by the methane vapor signal) reached a plateau value after 60 min.

pressure correction itself.

A third source of uncertainty in sample pressure comes from incomplete thermal equilibration during mixture preparation. The NMR sample cell was placed inside a nitrile glove and immersed in a water bath while it was pressurized with methane. After pressurization (and an additional 2 min for pressure stabilization) the cell was removed from the water bath and sealed (see Section 2.3.). In total, the cell was in the water bath about 10 min, at which point we estimate that it was within 0.5 K of the bath temperature. This temperature difference resulted in a relative standard uncertainty in the final pressure (after full thermal equilibration of the sealed cell) of about 0.16 %.

Quadrature addition of the three sources of uncertainty results in (relative) combined standard uncertainties in pressure that range from 0.16 % (for vapor-phase measurements at higher temperature-pressure combinations) to 0.52 % (for the liquid-phase measurement at the lowest temperature and pressure). Details of the uncertainty at each (T, p) state point are given in Table S2 in Appendix A.

#### 3. Results and discussion

Herein we describe VLE measurements made with <sup>1</sup>H NMR spectroscopy for mixtures of methane + water. Only proof-of-principle VLE measurements with this type of NMR-based method have been published previously (Suiter et al., 2020). Therefore, comparisons to published measurements and models for the VLE of methane + water are carefully considered to determine the reliability of the NMR-based approach. The two biggest challenges for these measurements were (1) to assure that the mixtures were at equilibrium before measurement and (2) to accurately integrate the disparately sized spectral peaks for the mixture components.

#### 3.1. Phase equilibration

Complete equilibration of the liquid and vapor phases is a prerequisite for VLE measurements. One advantage of NMR-based VLE measurements is that the approach to equilibrium can be monitored in real time without sample disturbance. However, the geometry of the NMR sample cell is not well suited to phase equilibration because of the small liquid-vapor interface (Suiter et al., 2020). Consequently, control experiments were performed to measure the approach to equilibrium in both vapor-phase and liquid-phase samples. The vapor phase equilibrates within about an hour without external perturbation, as shown in Fig. 6. Hence, after preparation, vapor-phase samples were immediately transferred into the NMR spectrometer for at least an hour of equilibration before beginning the NMR analysis. Conveniently, this is approximately the time needed to optimize spectral acquisition parameters (such as the manual shimming of the magnetic field).

Liquid-phase samples equilibrate much more slowly than vaporphase samples due to the taller liquid column and substantially slower diffusion in the liquid phase. As shown in Fig. 7, in the absence of mechanical mixing, the liquid phase does not reach equilibrium in 5 days. Fitting the data in Fig. 7 to a 1D diffusion model, (Yokozeki, 2002; Witherspoon and Saraf, 1965) suggests that full equilibration would take about 30 days. To speed equilibration, the liquid phase was mixed by adding glass beads to the sample cell and then rotating the sample cell during equilibration so that the beads repeatedly moved from one end of the liquid phase to the other (see Section 2.6. for details). With this mixing procedure, a liquid-phase sample at 299.73 K and 10.41 MPa reaches equilibrium after about 4000 half rotations (i.e., 180° rotations). For convenience, and out of an abundance of caution, all liquid-phase samples were allowed to equilibrate overnight (approximately 9600 half rotations and 18 h) before NMR analysis.

Slow equilibration of the methane + water mixtures made it necessary to seal the sample cell long before phase equilibration was complete. Fortunately, pressure changes that result from phase equilibration are relatively small because, at the temperatures and pressures studied,

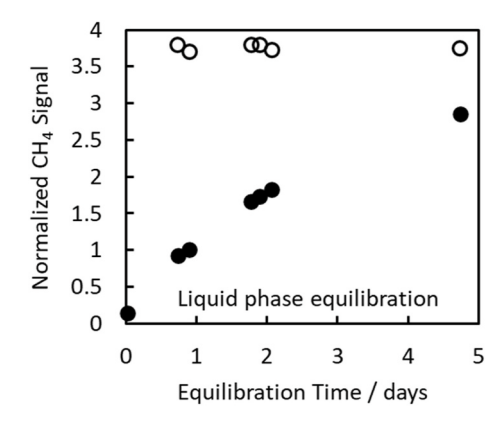


**Fig. 7.** Equilibration of the liquid phase for two samples of methane + water at 299.73 K and 10.41 MPa. The solid circles are for an experiment without mechanical mixing. The open circles are for an experiment in which the liquid phase was mixed with glass beads. The normalized methane signal was obtained by dividing by the liquid water signal.

 $\leq$ 1.8 % of the total methane dissolved in the liquid phase and the mole percent of water in the vapor phase never exceeded 1.1 %. Additionally, the dissolution of methane and evaporation of water partially offset each other. Based on the change in the number of molecules in the vapor phase (as determined from the NMR spectra), and assuming ideal mixture behavior, we applied a correction to the pressure setpoint to account for phase equilibration (see Section 2.7.). The magnitude of this correction never exceeds 1.6 % of the initial pressure. For liquid-phase samples, methane dissolution dominates, and the correction lowers the pressure. For vapor phase samples, water evaporation dominates, and the correction increases the pressure. The ability to do this type of correction with low uncertainty is one of the few advantages of the methane + water mixture from the standpoint of measuring its VLE behavior.

# 3.2. Integration of peak areas in the NMR spectra

The second major challenge in this work was to minimize uncertainty in the integration of peak areas. This was a challenge because of the large differences in the size of the two peaks and because of extensive peak overlap for the vapor-phase spectra.

In a properly configured <sup>1</sup>H NMR experiment, the spectral peak areas are directly proportional to the number of <sup>1</sup>H nuclei that contribute to the peak; therefore, mole fractions can be calculated directly from peak areas. However, the Lorentzian peak shapes observed in NMR spectroscopy extend to infinity. Consequently, it is necessary to correct for the fraction of the total peak intensity that is integrated with finite integral limits. It is also necessary to correct for peak overlap because every peak overlaps every other peak in the spectrum, although the extent of overlap is not always significant. A detailed protocol for making these two corrections-herein referred to as the "linewidths correction" and the "overlap correction"—has been published elsewhere, (Suiter et al., 2019) but the basic strategy is to set the integral limits for each peak based on the linewidth of the peak itself. Then, assuming a Lorentzian peak shape, it is straightforward to calculate the needed corrections. For the liquid-phase spectra, the water and methane peaks are well separated, as seen in Fig. 8, which allowed the use of our previously described integration strategy (Suiter et al., 2019) without modification.

Fig. 9 is a representative <sup>1</sup>H NMR spectrum of a vapor-phase sample. A comparison of Figs. 8 and 9 illustrates an important feature of NMR spectroscopy for VLE measurements: vapor-phase peaks appear in a different part of the spectrum than liquid-phase peaks (Suiter et al., 2020). Hence, condensation of water onto the wall of the NMR sample cell would not contribute to the vapor-phase peaks, which is a notable

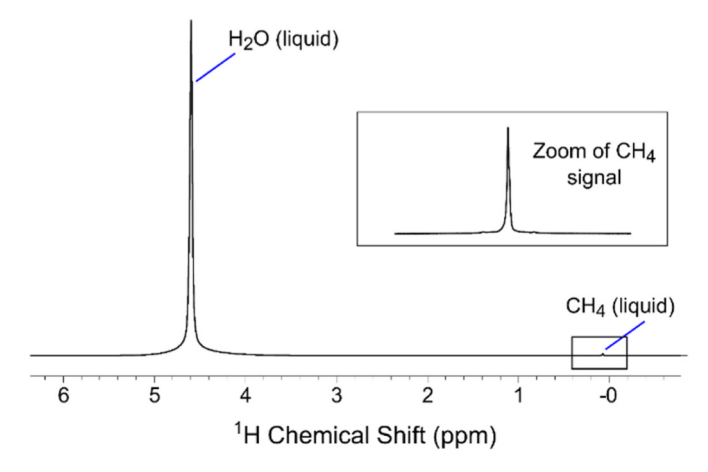


**Fig. 8.** A representative <sup>1</sup>H NMR spectrum for the liquid phase of the methane + water mixture at 307.98 K and 6.94 MPa. The large signal on the left is from liquid-phase water. The much smaller signal on the right is from liquid-phase (i. e., dissolved) methane. A vertically expanded region of the spectrum corresponding to the methane signal is shown for clarity.

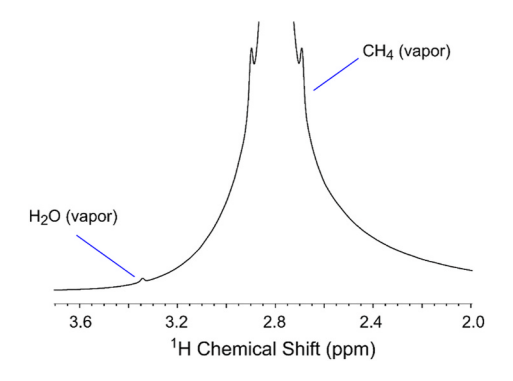


**Fig. 9.** A representative vapor-phase spectrum of methane + water at 307.98 K and 6.93 MPa. The small signal on the left is from vapor-phase water. The much larger signal on the right (cut off in the figure) is from vapor-phase methane. Overlap of the methane peak on the water peak complicates signal integration. Note that the symmetric shoulders on the methane peak near 2.7 ppm and 2.9 ppm are caused by natural abundance  $^{13}$ C.

# advantage of the NMR method.

Unfortunately, for the methane + water mixture, the vapor-phase peaks are not well separated. In fact, the vapor-phase water peak (at 3.34 ppm) forms a small bump on the sloping shoulder of the large, vapor-phase methane peak (at 2.80 ppm). In the vicinity of the water-vapor peak, the methane-vapor peak contributes more to the total signal intensity than the water-vapor peak itself. Hence, even with narrow integral limits, the integration strategy employed for the liquid-phase samples would result in an overlap correction for the water-vapor peak that is several times its corrected area. Consequently, a new peak integration strategy was devised, as described in detail in Section 2.5.2. In short, the water-vapor peak is integrated after an additional baseline subtraction to remove overlap from the sloping shoulder of the methane-vapor peak.

**3.3.** *VLE Measurements.* VLE measurements were made at 299.73 K, 307.98 K, and 323.25 K. At each temperature, mixtures were prepared at six pressures (nominally, 0.7 MPa, 1.8 MPa, 3.5 MPa, 6.9 MPa, 10.3 MPa, and 13.8 MPa). For each state point, two samples were prepared for <sup>1</sup>H NMR spectroscopy. One sample had a relatively large volume of water in the sample cell; this sample used to measure the liquid-phase composition (Table 2 and Fig. 10). The other sample had a relatively small volume of water in the sample cell; this sample was used to measure the vapor-phase composition (Table 3 and Fig. 11).

**Table 2** VLE measurements of temperature (T), pressure (p), and mole fraction of methane ( $x_{\text{methane}}$ ) for the liquid phase of methane + water mixtures.

T/K	p/MPa	$x_{ m methane}$
299.73	0.69	0.000115
	1.73	0.000352
	3.52	0.000662
	6.84	0.001347
	10.32	0.001853
	13.71	0.002100
307.98	0.71	0.000111
	1.76	0.000351
	3.45	0.000624
	6.94	0.001302
	6.84	0.001103
	6.82	0.001134
	6.81	0.001122
	10.30	0.001606
	13.71	0.001858
323.25	0.72	0.000110
	1.78	0.000295
	3.48	0.000573
	6.89	0.001055
	10.24	0.001432
	13.71	0.001793

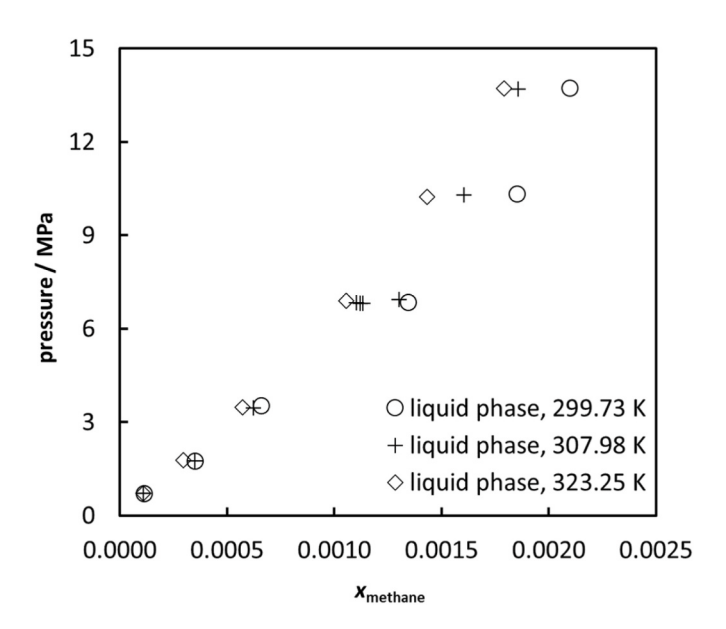


**Fig. 10.** Mole fraction of methane in the liquid phase  $(x_{\text{methane}})$  across the experimental temperature and pressure range.

For the temperature and pressure ranges of this work, the mole fraction of the minor component of each phase-methane in the liquid phase  $(x_{methane})$  or water in the vapor phase  $(y_{water})$ —is three to four orders of magnitude smaller than the mole fraction of the major component. As expected, higher pressures and lower temperatures yield larger values of  $x_{\text{methane}}$ . The opposite trends were observed for  $y_{\text{wa-}}$ ter-lower pressures and higher temperatures yield larger values of  $y_{\text{water}}$ . Larger values of  $x_{\text{methane}}$  and  $y_{\text{water}}$  have lower relative uncertainty because the associated NMR signals are larger. Thus,  $x_{\text{methane}}$  has the lowest relative uncertainty at the highest pressures and  $y_{water}$  has the lowest relative uncertainty at the lowest pressures (see Table 1). Measurements were repeated several times for both phases at 307.98 K and a nominal pressure of 6.9 MPa, Tables 2 and 3. Given that these conditions are in the middle of the temperature and pressure ranges, composition uncertainties are near their minimum for both phases. In each phase, one of the measurements appears to be an outlier, but we have no compelling reason to exclude these from the data set. Retaining the

**Table 3** VLE measurements of temperature (T), pressure (p), and mole fraction of water (y<sub>water</sub>) for the vapor phase of methane + water mixtures.

T/K	p/MPa *	$y_{ m water}$
299.73	0.76	0.002538
	1.78	0.001005
	3.46	0.000756
	6.97	0.000333
	10.41	0.000265
	13.80	0.000215
307.98	0.71	0.003969
	1.77	0.001819
	3.48	0.000989
	6.93	0.00070
	6.89	0.000559
	6.90	0.000509
	6.93	0.00049
	6.93	0.00051
	10.37	0.000378
	13.86	0.000319
323.25	0.71	0.00840
	1.76	0.00367
	3.53	0.002063
	6.93	0.000978
	10.39	0.000525
	13.89	0.000446

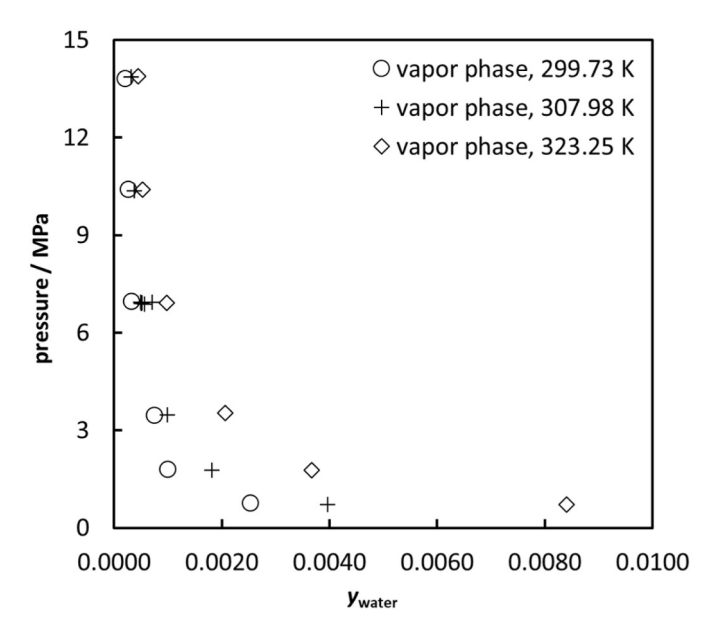


Fig. 11. Mole fraction of water in the vapor phase  $(y_{water})$  across the experimental temperature and pressure range.

"outlier" makes the standard deviation of repeat measurements about twice as large as the estimated uncertainties in mole fraction alone, although uncertainties in T and p also contribute to the scatter, as do small variations in pressure from sample to sample.

# 3.3. Comparison with literature measurements and models: liquid phase

The simplest thermodynamic model for liquid-phase composition in VLE is Henry's Law, which states that the concentration of dissolved gas is proportional to the partial pressure of the gas in the vapor phase (Sander, 2015). Of course, this linear relationship between partial pressure and concentration only holds at lower pressures. The proportionality constant, called the Henry's Law constant ( $k_{\rm H}$ ), has a temperature dependence that is typically reported as  $\frac{d(\ln k_{\rm H})}{d(1/T)}$ . We used consensus values from a recent literature review for the methane + water system:

 $k_H^0$  (298.15 K) = 1.4  $10^{-8}$  mol·(kg·Pa) $^{-1}$  and  $\frac{d(\ln k_H)}{d(1/T)}$  = 1700 K (Sander, 2015). As hoped, Henry's Law predictions of liquid-phase composition form a tangent to the lower-pressure, NMR-based, VLE measurements at 299.73 K (Fig. 12). Similar good agreement with Henry's Law is also observed for the NMR measurements at 307.98 K and 323.25 K (see Figs. S2 and S3 in Appendix A). This is an important confirmation that the NMR-based VLE measurements are reliable.

NMR-based measurements of the liquid phase composition are in notably poor agreement with the GERG-2008 thermodynamic model, (Kunz and Wagner, 2012) which dramatically underestimates the concentration of methane in the liquid phase (see the near-vertical red line in Fig. 12). This is not surprising because the GERG-2008 model is known to perform poorly for VLE predictions of water-rich mixtures (Herrig, 2018; Lemmon). This problem with the GERG-2008 model arises from limitations in the data used to develop the model and from the difficulty of modeling saturation boundaries for nearly pure fluid phases. More information about the GERG-2008 model and its implementation in the NIST REFPROP database (Lemmon et al., 2018) is outlined in Appendix A. The newer thermodynamic model by Herrig (2018) which includes a departure function absent from the GERG-2008 model, is clearly the best of the thermodynamic models for the methane + water mixture (Fig. 12), although it slightly overpredicts methane solubility at higher pressures.

NMR-based measurements of the liquid phase composition are in excellent agreement with existing experimental data (Frost et al., 2014; Kim et al., 2003; Chapoy et al., 2004; Awan et al., 2010; Wang et al., 1995; Yang et al., 2001). Fig. 12 shows experimental data near 300 K and Figs. S2 and S3 of Appendix A show a comparison of the NMR data with literature data near 310 K and 323 K, respectively. It has been pointed out previously (Herrig, 2018) that the data from Frost et al. (2014) are likely to be of the best quality in this temperature range. However, even the data from Frost et al., which were obtained by GC-FID and GC-TCD analysis of the liquid phase, lacks a detailed uncertainty analysis for the composition determination. The NMR-based measurements also compare well with existing data in terms of scatter, especially at the higher temperatures (see Figs. S2 and S3 in Appendix A).

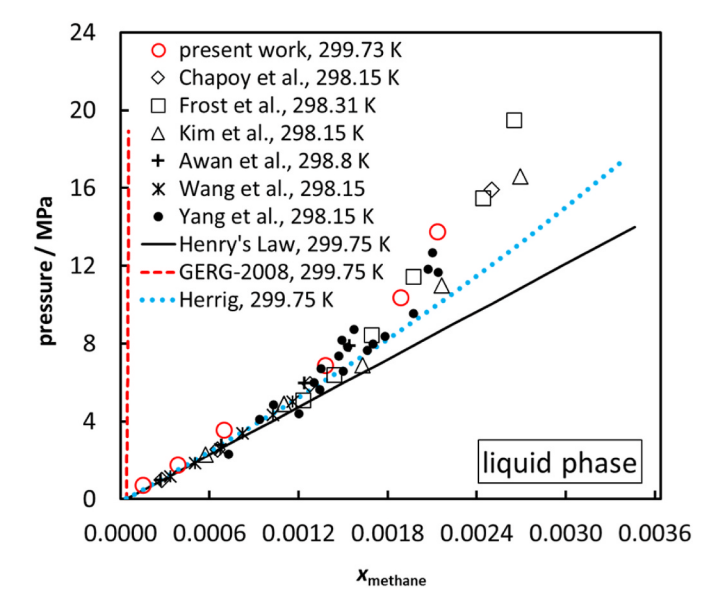


Fig. 12. A comparison of the present work to literature data (Frost et al., 2014; Kim et al., 2003; Chapoy et al., 2004; Awan et al., 2010; Wang et al., 1995; Yang et al., 2001) and models (Kunz and Wagner, 2012; Herrig, 2018) near 300 K for the liquid phase of the methane + water mixture.

#### 3.4. Comparison with literature measurements and models: vapor phase

NMR-based measurements of the vapor phase composition resulted in values of  $y_{\text{water}}$  that are lower than any of the other published data, (Rigby and Prausnitz, 1968; Frost et al., 2014; Mohammadi et al., 2006; Chapoy et al., 2005) and are about half of the predicted values from the GERG-2008 model (Kunz and Wagner, 2012) or the Herrig model (Herrig, 2018), Fig. 13. Similarly low values of  $y_{\text{water}}$  from the NMR-based measurement are also observed at the higher temperatures (see Figs. S4 and S5 of Appendix A). The relatively good agreement between the two models and the previously published data is expected. Herrig used all the data sets shown in Figs. 12 and 13 for model development. And the GERG-2008 model was developed for vapor-phase natural gas mixtures, so there is no surprise that it performs better for the vapor phase than for the liquid phase.

It is not clear why the NMR measurements yielded relatively low values of ywater. One possible explanation is that previously published measurements simply have large uncertainties in composition. Of the published data, only Rigby and Prausnitz (1968) provide careful uncertainty assessments for the composition measurement (Herrig, 2018). Another possible explanation is that there is some unidentified source of systematic error associated with NMR-based measurements on the vapor phase. Such an error would likely be associated with the integration of the heavily overlapped signals in the vapor-phase spectra (recall that there is only minor signal overlap in the liquid-phase spectra). We believe that this is the most likely explanation for the disagreement, given that the NMR-based method is new and is operating near its sensitivity limits. For example, the assumption of symmetric Lorentzian peak shapes combined with the baseline subtraction method used for the vapor phase spectra could lead to erroneously low integral values. The trustworthiness of the vapor-phase NMR measurements is unlikely to be resolved without a careful study of this specific scenario. Such a study would include careful preparation of vapor-phase mixtures of known composition where the mixture components have widely disparate concentrations and spectral signals with different degrees of overlap. This is a labor-intensive undertaking that is well beyond the scope of the current work but is a future study we plan to attempt. If the vapor-phase NMR measurements do prove reliable, there would be important, practical implications for the operation of natural gas pipelines and related infrastructure. Specifically, the NMR measurements suggest that the "carrying capacity" of the vapor phase for water is only about half of what the current models suggest. Thus, a deleterious aqueous phase would form more readily than currently expected.

#### 4. Conclusions

For difficult measurements, the use of multiple measurement methods is desirable because it is the most reliable path to understanding data quality. In this regard, NMR spectroscopy is a useful complement to more traditional VLE measurement methods such as GC. For the liquid-phase measurements on the methane + water mixture, the results from NMR spectroscopy agree with traditional methods and, based on scatter and agreement with Henry's Law, show evidence of being similar in quality to the best available measurements. For vaporphase measurements, NMR spectroscopy yields systematically lower values of ywater across all measured temperatures and pressures for reasons that remain unclear. As part of the work on methane + water mixtures, we made two notable advances in the use of NMR spectroscopy for VLE measurements. First, we developed a method by which the vapor-phase and liquid-phase compositions are measured in separate experiments. This was done by preparing two samples with different amounts of the liquid phase so that the vapor phase or the liquid phase occupied the entire active volume of the spectrometer. Second, we developed a novel mixing protocol to hasten phase equilibration. This was accomplished with the addition of glass beads to the NMR sample cell in combination with automated rotation of the cell at the desired

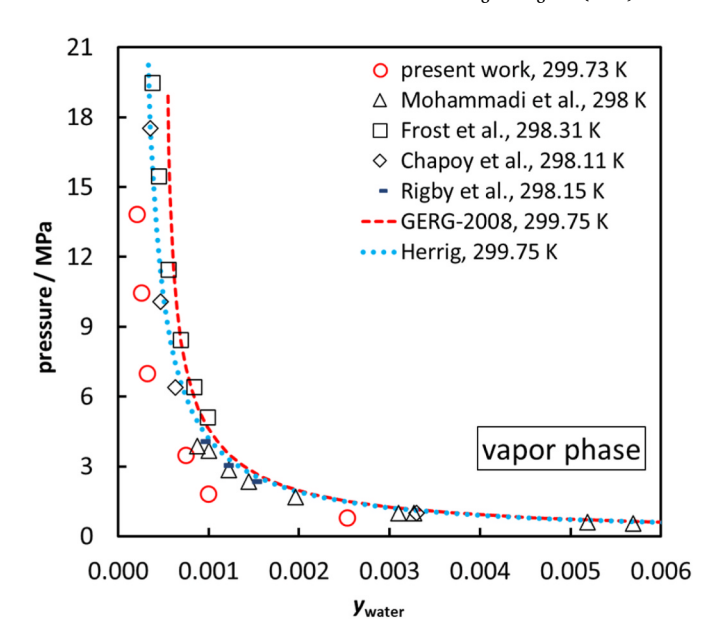


**Fig. 13.** Comparison of the present work to literature data (Rigby and Prausnitz, 1968; Frost et al., 2014; Mohammadi et al., 2006; Chapoy et al., 2005) and models (Kunz and Wagner, 2012; Herrig, 2018) near 300 K for the vapor phase of the methane + water mixture.

temperature and pressure. We believe that these two strategies will be applicable to measurements on many other mixtures.

# CRediT authorship contribution statement

Samantha L. Miller: Validation, Formal analysis, Investigation, Writing – review & editing, Visualization. Michael Sartini: Methodology, Formal analysis, Investigation, Writing – original draft, Visualization. Bret C. Windom: Conceptualization, Writing – original draft, Writing – review & editing, Project administration, Funding acquisition. Christopher L. Suiter: Methodology, Validation, Formal analysis, Investigation, Writing – review & editing. Mark O. McLinden: Conceptualization, Writing – review & editing. Nancy E. Levinger: Writing – review & editing, Supervision. Jason A. Widegren: Conceptualization, Resources, Writing – review & editing, Project administration.

#### Declaration of competing interest

The authors declare the following financial interests/personal relationships which may be considered as potential competing interests: Bret C. Windom and Michael Sartini report financial support was provided by Southern Gas Association, Gas Machinery Research Council. Samantha L. Miller reports financial support was provided by National Science Foundation.

# Data availability

Data will be made available on request.

## Acknowledgement

We thank Dr. Ian Bell for implementation of the GERG-2008 model and the Herrig model. SLM gratefully acknowledges support by an INTERN supplement to NSF CHE grant number 1956323. BCW and MS gratefully acknowledge support from the Gas Machinery Research Council (Southern Gas Association).

#### Appendix B. Supplementary data

Supplementary data to this article can be found online at https://doi.org/10.1016/j.jgsce.2023.205165.

#### References

- Awan, J.A., Thomsen, K., Coquelet, C., Fosbol, P.L., Richon, D., 2010. Vapor-liquid equilibrium measurements and modeling of the propyl mercaptan + methane + water system. J. Chem. Eng. Data 55, 842–846.
- Budiman, H., Nuryatini, Zuas, O., 2015. Comparison between GC-TCD and GC-FID for the determination of propane in gas mixture. Procedia Chem. 16, 465–472.
- Chapoy, A., Mohammadi, A.H., Richon, D., Tohidi, B., 2004. Gas solubility measurement and modeling for methane-water and methane-ethane-n-butane-water systems at low temperature conditions. Fluid Phase Equil. 220, 113–121.
- Chapoy, A., Coquelet, C., Richon, D., 2005. Corrigendum to "Revised solubility data and modeling of water in the gas phase of the methane/water binary system at temperatures from 283.08 to 318.12 K and pressures up to 34.5 MPa". Fluid Phase Equil. 230, 210–214.
- Claridge, T.D.W., 2009. High-Resolution NMR Techniques in Organic Chemistry, second ed. Elsevier, Amsterdam.
- Cosgrove, B.A., Walkley, J., 1981. Solubilities of gases in H<sub>2</sub>O and <sup>2</sup>H<sub>2</sub>O. J. Chromatogr. A 216, 161–167.
- Frost, M., Karakatsani, E., von Solms, N., Richon, D., Kontogeorgis, G.M., 2014.
  Vapor–liquid equilibrium of methane with water and methanol. Measurements and modeling. J. Chem. Eng. Data 59, 961–967.
- Hall, K., Yarborough, L., 1973. A new equation of state for Z-factor calculations. Oil Gas J. 71, 82–92.
- Herrig, S., 2018. New Helmholtz-Energy Equations of State for Pure Fluids and CCS-Relevant Mixtures. Ruhr-Universität Bochum, Bochum.
- Hughes, T.J., Guo, J.Y., Baker, C.J., Rowland, D., Graham, B.F., Marsh, K.N., Huang, S. H., May, E.F., 2017. High pressure multi-component vapor-liquid equilibrium data and model predictions for the LNG industry. J. Chem. Thermodyn. 113, 81–90.
- Jafar Mazumder, M.A., 2020. Global impact of corrosion: occurrence, cost and mitigation. Glob. J. Eng. Sci. 5, 1-5
- Kidnay, A.J., Parrish, W.R., 2006. Fundamentals of Natural Gas Processing. Taylor & Francis Group, Boca Raton.
- Kim, Y.S., Ryu, S.K., Yang, S.O., Lee, C.S., 2003. Liquid Water–Hydrate equilibrium measurements and unified predictions of hydrate-containing phase equilibria for methane, ethane, propane, and their mixtures. Ind. Eng. Chem. Res. 42, 2409–2414.
- Kunz, O., Wagner, W., 2012. The GERG-2008 wide-range equation of state for natural gases and other mixtures: an expansion of GERG-2004. J. Chem. Eng. Data 57, 3032–3091.

- Lemmon, E.W., Bell, I.H., Huber, M.L., McLinden, M.O., 2018. NIST Standard Reference Database 23: Reference Fluid Thermodynamic and Transport Properties-REFPROP, Version 10.0. National Institute of Standards and Technology, Gaithersburg, MD.
- Lemmon, E. W. Irregularities in calculations or plots for mixtures containing water #298: https://github.com/usnistgov/REFPROP-issues/issues/298. (accessed February 2023).
- Menon, S., Ganti, H., Niemeyer, K.E., Hagen, C., 2017. Effects of oil and water contamination on natural gas engine combustion processes. J. Nat. Gas Sci. Eng. 41, 30–39.
- Mohammadi, A.H., Chapoy, A., Tohidi, B., Richon, D., 2006. Gas solubility: a key to estimating the water content of natural gases. Ind. Eng. Chem. Res. 45, 4825–4829.
- Popoola, L.T., Grema, A.S., Latinwo, G.K., Gutti, B., Balogun, A.S., 2013. Corrosion problems during oil and gas production and its mitigation. Int. J. Ind. Chem. 4, 35.
- Richon, D., de Loos, T.W., 2005. Vapour-liquid equilibrium at high pressure. In: Weir, R. D., de Loos, T.W. (Eds.), Measurement of the Thermodynamic Properties of Multiple Phases, International Union of Pure and Applied Chemistry.
- Rigby, M., Prausnitz, J.M., 1968. Solubility of water in compressed nitrogen, argon, and methane. J. Phys. Chem. 72, 330–334.
- Sander, R., 2015. Compilation of Henry's law constants (version 4.0) for water as solvent. Atmos. Chem. Phys. 15, 4399–4981.
- Sharanik, J., Duri, M., Hadjistassou, C., 2023. Liquefied natural gas (LNG). In: Reference Module in Biomedical Sciences. Elsevier, Amsterdam.
- Shi, S., Han, G., Zhong, Z., Li, Z., 2021. Experimental and simulation studies on the slug flow in curve pipes. ACS Omega 6, 19458–19470.
- Sotak, C.H., Dumoulin, C.L., Levy, G.C., 1983. Software for quantitative analysis by carbon-13 fourier transform nuclear magnetic resonance spectrometry. Anal. Chem. 55, 782–787.
- Suiter, C.L., McLinden, M.O., Bruno, T.J., Widegren, J.A., 2019. Composition determination of low-pressure gas-phase mixtures by H-1 NMR spectroscopy. Anal. Chem. 91, 4429–4435.
- Suiter, C.L., Malavé, V.D., Garboczi, E.J., Widegren, J.A., McLinden, M.O., 2020. Nuclear magnetic resonance (NMR) spectroscopy for the in situ measurement of vapor–liquid equilibria. J. Chem. Eng. Data 65, 3318–3333.
- Tamalmani, K., Husin, H., 2020. Review on corrosion inhibitors for oil and gas corrosion issues. Appl. Sci. 10.
- Wang, Y.L., Han, B.X., Yan, H.K., Liu, R.L., 1995. Solubility of CH<sub>4</sub> in the mixed solvent tbutyl alcohol and water. Thermochim. Acta 253, 327–334.
- Wilhelm, E., Battino, R., Wilcock, R.J., 1977. Low-pressure solubility of gases in liquid water. Chem. Rev. 77, 219–262.
- Witherspoon, P.A., Saraf, D.N., 1965. Diffusion of methane, ethane, propane, and n-butane in water from 25 to 43 degrees. J. Phys. Chem. 69, 3752–3755. Yang, S.O., Cho, S.H., Lee, H., Lee, C.S., 2001. Measurement and prediction of phase
- Yang, S.O., Cho, S.H., Lee, H., Lee, C.S., 2001. Measurement and prediction of phase equilibria for water plus methane in hydrate forming conditions. Fluid Phase Equil. 185, 53–63.
- Yokozeki, A., 2002. Time-dependent behavior of gas absorption in lubricant oil. Int. J. Refrig. 25, 695–704.